PROCEEDINGS OF THE SIXTH BIOMECHANICS SEMINAR

1992

Editor: Christian Högfors
Gunnar Andréasson

CENTRE FOR BIOMECHANICS
Chalmers University of Technology
and
Gothenburg University

Biomech. Sem. vol 6, (1992) ISSN 1100-2247

Numerical Calculation of Navier-Stokes Equations in Biological Ducts

Bijan Farhanieh and Lars Davidson
Department of Thermo - and Fluid Dynamics, Chalmers University of Technology 412 96 Göteborg, Sweden

Abstract

A body-fitted-finite-volume scheme for calculations of Navier-Stokes equations in complex three dimensional geometries are presented. This method also utilizes collocated variables and cartesian velocity components. The problem of non-physical oscillation in pressure and velocity fields is overcome by introducing the Rhie-Chow interpolation procedure. The performence of the code is assessed by comparing the calculated results of flow characteristic through a sever stenosis with available experimental data.

1 Introduction

Some deseases effect the flow of cerebrospinal fluids, and of urine, and artificial valves and other devices which are introduced into the body as remedies. The efficiency of these can be predicted, and their design and location optimised by simulating the flow phenomena within them, and within the biological ducts and issues with which they are connected. There are also some disorders of the circulatory system which are belived to be associated with fluid flow phenomena in the vicinity of branches and junctions. The flow simulation capability of the available computer codes allows hypotheses to be investigated and danger spots to be resealed.

The objective of this paper is to describe the employment of a body-fitted finite-volume code with a collocated variable arrangement which is capable of simulating fluid flow in three-dimensional complex geometries.

An important advantage of this method (collocated variable arrangement) is that the control volume for all variables coincide with the boundaries of the solution field and therefore simplifies the specification of the boundary conditions in complex geometries.

The computation is based upon the solution of the partial differential equations governing the flows. The equations are written in non-orthogonal coor-

dinate system. The finite - volume method is applied to transform the partial differential equations to algebraic relations which link the values of the dependent variables at the nodes of the computational grid. The TDMA (Tri-Diagonal Matrix Algorithm) is then adapted to solve the obtained algebraic relations. Two different differencing schemes are available to approximate the convective fluxes: Hybrid central/upwind differencing or the van Leer scheme. SIMPLEC [1] handles the linkage between velocities and pressure.

The Cartesian velocity components are used in the program. This method have been used by Shyy *et al.*[2] and Braaten and Shyy [3]. In contrast to most of the finite volume codes which use the conventional method of staggered grids for the velocity components, the present code utilizes the collocated variable arrangement in which all variables are stored at the same control volume. This arrangement has various advantages over the staggered grid, e.g. the control volumes for all variables coincide with the boundaries of the solution domain, facilitating the specification of boundary conditions, and geometrical data need to be calculated only for one set of control volumes (when staggered arrangement is used the geometrical data must be calculated for four sets of control volume).

The code can be applied to axi-symmetric and plane flows. The boundaries in a flow can be a wall, a plane or axis symmetry or a boundary along which the values of the dependent variables are prescribed.

The performance of the code is assessed by computation of fluid flow through a stenosis. The code is used for solving the governing equation system.

2 Solution Methodology

In order to extend the capabilities of the finite difference method to deal with complex geometries, a boundary fitted coordinate method is used.

The basic idea in this method is to map the complex flow domain in the physical space to a simple rectangular domain in the computational space by using a curvilinear coordinate transformation. In other words, the Cartesian coordinate system x_i in the physical domain is replaced by a general non-orthogonal system ξ_i.

The momentum equations are solved for the velocity components U, V, W in the fixed Cartesian directions on a non-staggered grid. This means that all the variables are stored at the center of the control volume. This method was suggested and worked out by Rhie and Chow [4] and later used by Burns and Wilkes [5], Majumdar [6], Peric *et al.*[7] and Miller and Schmidt [8]. Ma-

jumdar [9] later discussed the importance of underrelaxation in momentum interpolation when non-staggered grids are used.

The steady transport equation for a general dependent variable Φ in the Cartesian coordinates can be written as

$$\frac{\partial}{\partial t}(\rho\Phi) + \frac{\partial}{\partial x_i}(\rho U_i \Phi) = \frac{\partial}{\partial x_i}\left(\Gamma_\Phi \frac{\partial \Phi}{\partial x_i}\right) + S \tag{1}$$

where Γ_Φ is the exchange coefficient and is equal to viscosity in the momentum equations. The independent variable Φ can be equal U, V, W, P' etc.

The total flux, convective and diffusive fluxes, is defined as

$$I_i = \rho U_i \Phi - \Gamma_\Phi \frac{\partial \Phi}{\partial x_i} \tag{2}$$

It is now convenient to write eq. (2) in the equivalent form

$$\frac{\partial I_i}{\partial x_i} = S_\phi \tag{3}$$

Integration of eq. (3) over any control volume in the physical space, using Gauss' law, gives

$$\int_A \vec{I} \cdot d\vec{A} = \int_V S_\phi dV \tag{4}$$

Equations (3) and (4) are used for performing the transformation to the computational space coordinates (general non-orthogonal coordinates) ξ_i.

The scalar advection - diffusion equation 4 is discretized. The integration of this gives

$$\left(\vec{I}\cdot\vec{A}\right)_e + \left(\vec{I}\cdot\vec{A}\right)_w + \left(\vec{I}\cdot\vec{A}\right)_n + \left(\vec{I}\cdot\vec{A}\right)_s + \left(\vec{I}\cdot\vec{A}\right)_h + \left(\vec{I}\cdot\vec{A}\right)_l = S\delta V \tag{5}$$

where e, w, n, s, h and l refer to the faces of the control volume, see *Fig.*1. The discretized equation is rearranged in the standard form

$$a_P \Phi_P = \sum a_{NB} \Phi_{NB} + S_C \tag{6}$$

where

$$a_P = \sum a_{NB} - S_P \tag{7}$$

The coefficients a_{NB} contains the contribution due to convection and diffusion and the source terms S_P and S_C contains the remaining terms.

2.1 Convection

For the sake of conciseness and simplicity we restrict ourself in this and the following sub-sections only to the east face of the control volume for explanation of the numerical procedure. The total flux $\vec{I}$ contains convective and

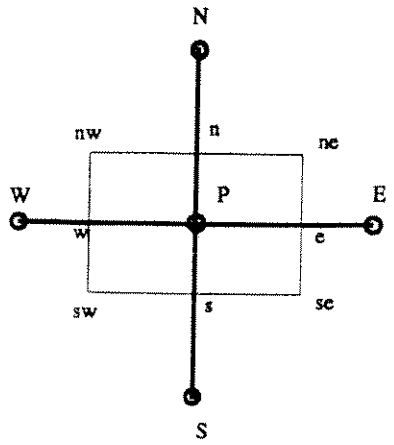

Figure 1: Control volume

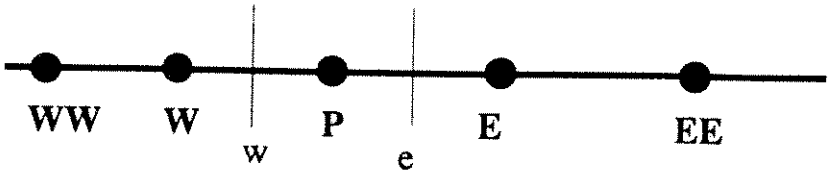

Figure 2: Grid nomenclature

diffusive fluxes. The first term in the right-hand side of eq. (2) is the convective term. The mass flow rate through the east face can be expressed as the scalar product of the velocity and area vectors multiplied by the density. Thus we have

$$\dot{m}_e = \rho_e \vec{U}_e \cdot \vec{A}_e = \rho_e \left(U_e A_{ex} + V_e A_{ey} + W_e A_{ez}\right) \tag{8}$$

where the Cartesian areas are calculated by

$$A_{ex} = \mid \vec{A} \mid_e \vec{n} \cdot e_x; \quad A_{ey} = \mid \vec{A} \mid_e \vec{n} \cdot e_y; \quad A_{ez} = \mid \vec{A} \mid_e \vec{n} \cdot e_z \tag{9}$$

where $\mid \vec{A} \mid_e$ is the total area of the east face, $\vec{n}$ its normal vector and $\vec{e}$ the Cartesian base vectors. In order to obtain the velocity components on the control volume faces from those on the control volume centers, the Rhie-Chow [4] interpolation method is used. In this method the weighted linear interpolation in physical space, $U_e = f_x U_E + (1 - f_x) U_P$, is not used in order to avoid non-physical oscillations in pressure and velocity. The method can be described as follows: Consider the interpolation to the east face of a control volume centered P, see *Fig.*2. The pressure gradient is subtracted from the velocity components stored at the center of the control volumes

$$\hat{U}_P = U_P - \frac{-(P_e - P_w)\,\delta V}{\mid \vec{we} \mid (a_P)_P} \qquad \textit{and} \qquad \hat{U}_E = U_E - \frac{-(P_{ee} - P_e)\,\delta V}{\mid e(\vec{ee}) \mid (a_P)_E} \tag{10}$$

The velocity components on the east face is now calculated as

$$U_e = f_x \hat{U}_E + (1 - f_x)\,\hat{U}_P + \text{Pressure gradient} \tag{11}$$

$$U_e = f_x \hat{U}_E + (1 - f_x)\,\hat{U}_P - \frac{-(P_E - P_P)\,\delta V}{|\,\vec{PE}\,|\,(a_P)_e} \tag{12}$$

where f_x is the interpolation factor and calculated by

$$f_x = \frac{|\,\vec{Pe}\,|}{|\,\vec{Pe}\,| + |\,\vec{eE}\,|} \tag{13}$$

P_e, P_w, P_{ee} in eq. (10) are calculated by linear interpolation. As seen from eq. (12) the pressure gradient is now calculated using the adjacent nodes of the east face. This avoids any non-physical oscillations in the pressure field. V_e and W_e are calculated in a similar manner.

The convective fluxes can be calculated by two different methods. These methods are briefly presented below.

2.1.1 Hybrid Upwind/Central Differencing Scheme

This scheme approximates the convective terms using a central differencing scheme if the local grid Reynolds number is below two, and otherwise upwind differencing, see *Fig.*2.

$$\Phi_w = \Phi_W, \quad \text{if} \quad |\,Re_{\delta x}\,| > 2 \quad \text{and} \quad U_w > 0 \tag{14}$$

$$\Phi_w = \Phi_P \quad \text{if} \quad |\,Re_{\delta x}\,| > 2 \quad \text{and} \quad U_w < 0 \tag{15}$$

$$\Phi_w = f_x \Phi_P + (1 - f_x)\,\Phi_W \quad \text{if} \quad |\,Re_{\delta x}\,| < 2 \tag{16}$$

where f_x is an interpolation factor equal to 0.5 if the face w lies midway between W and P.

2.1.2 The Van Leer Scheme

This scheme of Van Leer [10] is of second order accuracy, except at local minima or maxima where its accuracy is of first order. One advantage for this scheme is that it is bounded.

For face west it can be written, see *Fig.*2

$$\begin{aligned}
U_w &> 0 \\
\text{if } |\,\Phi_P - 2\Phi_W + \Phi_{WW}\,| &\geq |\,\Phi_P - \Phi_{WW}\,| \Longrightarrow \Phi_w = \Phi_W \\
\text{else } \Phi_w &= \Phi_W + \frac{(\Phi_P - \Phi_W)(\Phi_W - \Phi_{WW})}{\Phi_P - \Phi_{WW}} \\
U_w &< 0 \\
\text{if } |\,\Phi_W - 2\Phi_P + \Phi_E\,| &< |\,\Phi_W - \Phi_E\,| \Longrightarrow \Phi_w = \Phi_P \\
\text{else } \Phi_w &= \Phi_P + \frac{(\Phi_W - \Phi_P)(\Phi_P - \Phi_E)}{\Phi_W - \Phi_E}
\end{aligned}$$

This scheme is thus a first - order upwind with a correction term which gives it second order accuracy.

2.2 Diffusion

The second term in the total flux $\vec{I}$ presented in eq. (2), is the diffusion term. Through an area $\vec{A}$ we have

$$\left(\vec{I}\cdot\vec{A}\right)_{diff} = -\Gamma\vec{A}\cdot\nabla\Phi \tag{17}$$

$\vec{A}\cdot\nabla\Phi$ in eq. (17) can for the east face be rewritten in Cartesian coordinates as

$$\left(-\vec{A}\cdot\nabla\Phi\right)_e = -\left(A_{ex}\frac{\partial\Phi}{\partial x} + A_{ey}\frac{\partial\Phi}{\partial y} + A_{ez}\frac{\partial\Phi}{\partial z}\right)_e \tag{18}$$

and in general non-orthogonal coordinates

$$\left(-\vec{A}\cdot\nabla\Phi\right)_e = -\left(\vec{A}\cdot\vec{g}_i g^{ij}\frac{\partial\Phi}{\partial\xi_j}\right)_e = -\left(\mid\vec{A}\mid\vec{n}\cdot\vec{g}_i g^{ij}\frac{\partial\Phi}{\partial\xi_j}\right)_e \tag{19}$$

where $\vec{g}_i$ is the covariant (tangent) base vector. The appearance of the metric tensor, g_{ij} in eq. (19), is due to the fact that the components of the product $\vec{A}\cdot\vec{g}_i$ and the derivative $\frac{\partial\Phi}{\partial\xi_j}$ are both covariant and the product of their contravariant base vectors is not zero for $i \neq j$ since they are non-orthogonal to each other. The components of g^{ij} can be calculated as shown in e.g. [11].

The normal vector $\vec{n}$ in eq. (19) is equal to the cross product of $\vec{g}_2$ and $\vec{g}_3$ which implies that $\vec{n}\cdot\vec{g}_2 \equiv \vec{n}\cdot\vec{g}_3 = 0$. Eq. (19) can now be written as

$$\left(-\vec{A}\cdot\nabla\Phi\right)_e = -\left(\mid\vec{A}\mid\vec{n}\cdot\vec{g}_1 g^{1j}\frac{\partial\Phi}{\partial\xi_j}\right)_e \tag{20}$$

The diffusion can be written

$$\left(-\vec{A}\cdot\nabla\Phi\right)_e = D_{e\xi}\left(\Phi_E - \Phi_P\right) + D_{e\eta}\left(\Phi_{en} - \Phi_{es}\right) + D_{e\zeta}\left(\Phi_{eh} - \Phi_{el}\right) \tag{21}$$

where the geometrical arrays $D_{e\xi}$, $D_{e\eta}$ and $D_{e\zeta}$ are calculated once and stored.

2.3 Pressure correction equation

The pressure correction equation is obtained by applying the SIMPLEC algorithm [12] on the non-staggered grid. The mass flux $\dot{m}$ is divided into one old value, $\dot{m}^*$, and another correction value, $\dot{m}'$,. The mass flux correction at the east face can be calculated by

$$\dot{m}'_e = \left(\rho\vec{A}\cdot\vec{U}'\right)_e = \rho_e\left(A_{ex}U'_e + A_{ey}V'_e + A_{ez}W'_e\right) = \left(\rho\vec{A}\cdot\vec{g}^j U'_j\right)_e \tag{22}$$

where U_j' is the covariant correction velocity. The covariant velocity components are related to the pressure gradient [13]

$$U_j' = -\frac{\delta v}{a_P}\frac{\partial p}{\partial x_j} \tag{23}$$

By introducing eq. (22) into eq. (23) we obtain

$$\dot{m}' = \left[\rho\vec{A}\cdot\left(-\frac{\delta v}{a_P}\frac{\partial p}{\partial x_j}\vec{g}^j\right)\right]_e = -\left[\frac{\delta v\rho}{a_P}\vec{A}\cdot\nabla p'\right] \tag{24}$$

Consider, for simplicity, the continuity equation in one dimension

$$\dot{m}_e - \dot{m}_w = 0 \tag{25}$$

If $\dot{m} = \dot{m}^* + \dot{m}'$ and eq. (24) are substituted into eq. (25) we obtain

$$\left[\frac{\delta v\rho}{a_P}\vec{A}\cdot\nabla p'\right]_w - \left[\frac{\delta v\rho}{a_P}\vec{A}\cdot\nabla p'\right]_e + \dot{m}_e^* - \dot{m}_w^* = 0 \tag{26}$$

This is a diffusion equation for the pressure correction p'. $\vec{A}\cdot\nabla p'$ can be calculated with eq. (20) by replacing Φ by p'.

3 Case study - Flow characteristics in vascular stenosis

The partial occlusion of arteries due to stenotic obstruction is one of the most frequently occuring abnormalities in man. The development of localized arterial stenosis may lead to disordered blood flow within and downstream of the constricted region. Therefore, the ability to describe flow through a partial occlusion adds to the insight needed to solve the problem of the pathology of atherosclerosis. There is also widespread interest in determining whether the disordered flow patterns can be used to detect localized arterial disease in its early stages, particularly before it becomes clinically significant.

3.1 Geometry of stenosis

The numerical calculation is applied to axisymetric configuration which has the form described as

$$\frac{R}{R_o} = 1 - \frac{1}{3}[1 + cos(\frac{\pi x}{x_o})] \qquad for\ |x| \le x_o \tag{27}$$

$$\frac{R}{R_o} = 1 \qquad \text{for } |x| > x_o \tag{28}$$

The schematic diagram of the stenosis and the computational domain is presented in *Fig.* 3.

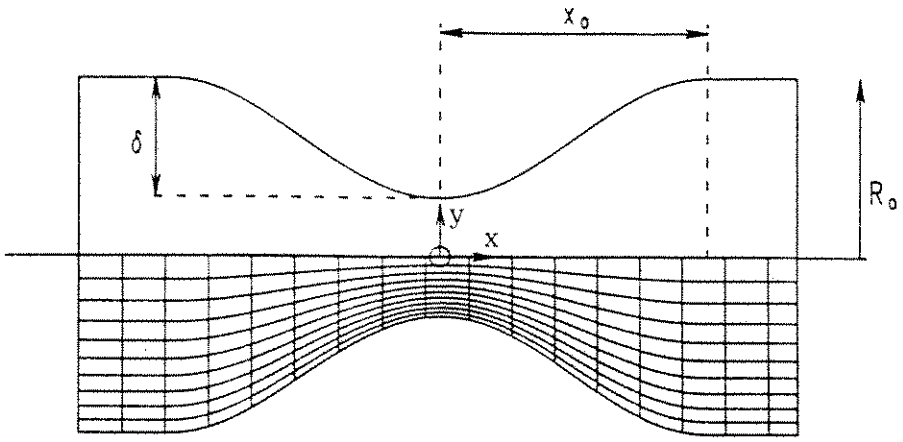

Figure 3: Schematic diagram of the stenosis (not to scale) and computational domain.

3.2 Convergence

The computations were performed for the Reynolds number ranging from 50 to 900. The computations were terminated when the sum of absolute residuals normalized by the inflow fluxes was below 10^{-4} for all the variables. The under-relaxation factors of 0.5 were chosen for the velocities and pressure correction. Upto 1000 iterations, depending on the Reynolds number, were required to obtain a converged solution. All calculations were carried out on a DEC 3100 work-station.

3.3 Flow field

A description of the various possible steady laminar flow patterns which may be encountered is best rendered by display of streamlines and velocity vectors for representative conditions. *Fig.* 4 illustrates curves of constant stream function as well as velocity vectors for two different Reynolds numbers in the region of a more severe stenosis. At these Reynolds numbers laminar separation takes place. The eddies containing recirculating fluid can be clearly observed as illustrated in the figure. The flow is laminar both outside and within the separated region. As the Reynolds number was increased the separated flow region extended for a considerable distance downstream.

The calculated points of separation and reattachment for $Re = 50$ and 100 are compared and listed in *Table* 1 with the experimental data of Young and Tsai [14], and calculated results of Karki [15], Deshpande *et al.*[16], Rastogi [17] and Davidson and Hedberg [18].

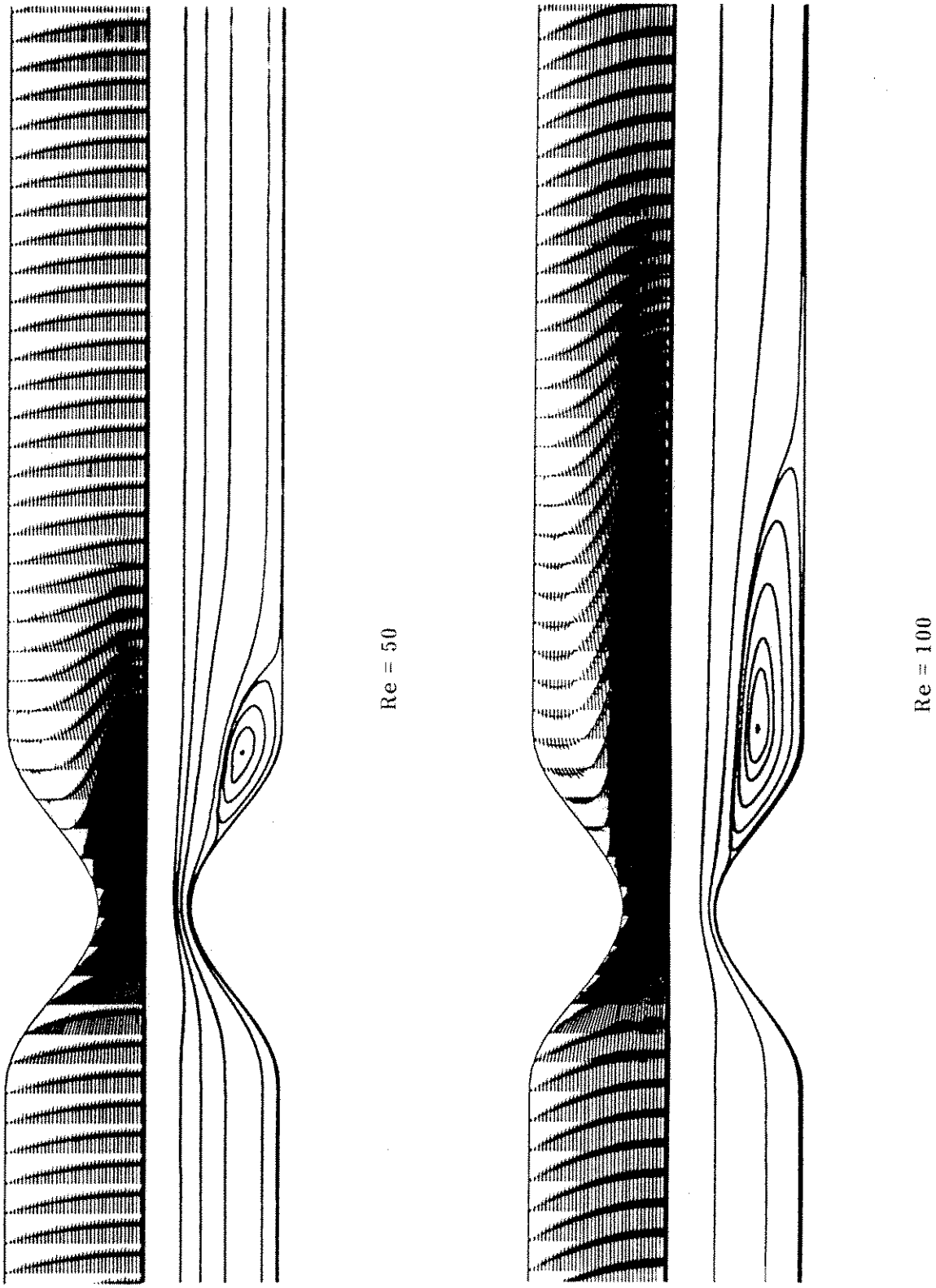

Figure 4: Streamlines and velocity vectors.

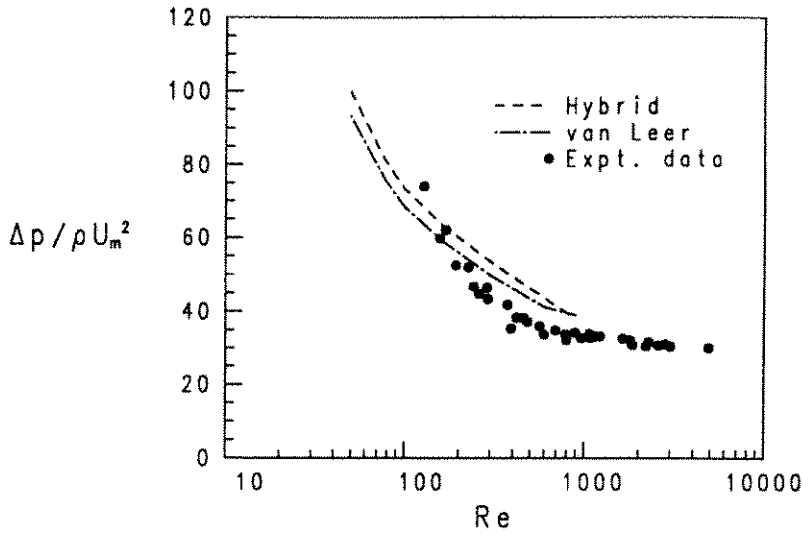

Figure 5: Pressure drop across stenosis.

Table 1 Points of separation and reattachment

Source of data	$Re = 50$ x_s/x_o, x_r/x_o	$Re = 100$ x_s/x_o, x_r/x_o
Young and Tsai (Expt.)[14]	0.37, 2.2	0.37, 4.0
Karki [15]	0.35, 2.1	0.35, 4.0
Deshpande *et al.*[16]	0.35, 2.1	0.35, 4.2
Rastogi [17]	-	0.35, 3.8
Davidson and Hedberg [18]	0.35, 2.07	0.31, 3.75
Present work (hybrid)	0.38, 2.04	0.38, 3.83
Present work (van Leer)	0.38, 2.04	0.38, 4.08

3.4 Pressure drop

Since the presence of a stenosis increases the resistance which the flow experiences and in the case of severe stonoses the region of the blood supply reduces considerably, the pressure losses through such constrictions are of physiologic interest.

The comparison of the pressure drop across stenosis with the experimental data is presented in *Fig.* 5. The convective fluxes were computed by two different method, Hybrid scheme and van Leer scheme. As seen from *Fig.* 5 the predicted result by the van Leer scheme is in better agreement with the experimental data. This scheme was used throughout the computations.

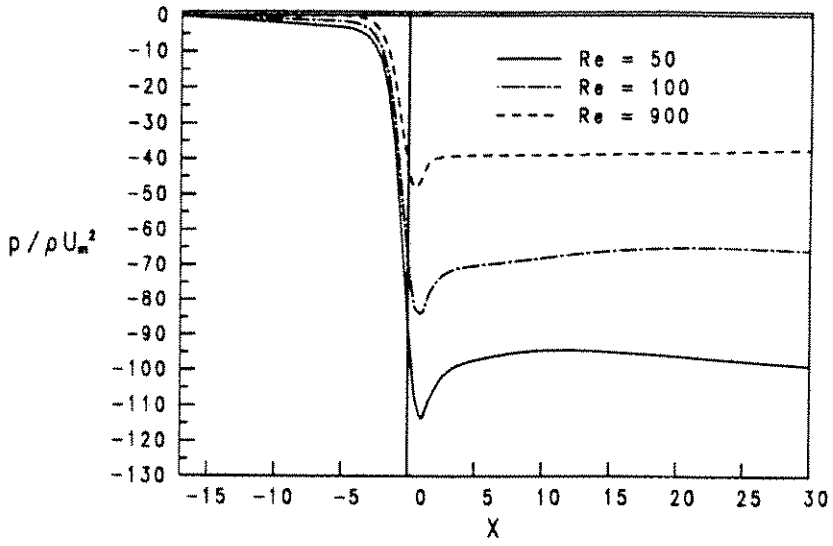

Figure 6: Pressure distribution along the duct.

The pressure distribution along the tube is also of interest. *Fig.* 6 presents the variation of pressure along the axis for the considered stenosis. There is a rapid fall in pressure as the occlusion is approached, and for this case a local minimum in the pressure is obtained just prior to the separation point. The calculations show a recovery of the pressure gradient far downstream to the fully developed pipe flow result.

3.5 Flow velocities

The velocity profiles are also of interest since they provide a detailed description of the flow field. *Fig.* 4 illustrates the velocity vectors which give a comperhensive picture of the velocity profiles. The regions of reverse flow are clearly seen. The velocity vectors undergo a change of sign within the recirculation zone, indicating strong elliptic nature of the problem.

The variation of centerline velocity with axial location is presented in *Fig.* 7 for three representative Reynolds numbers. The recirculation zone is experianced by these three Reynolds numbers. As expected the point of reattachment moves downstream as the Reynolds number is increased.

4 Conclusions

This paper presents a finite-volume calculation procedure for computation of incompressible elliptic flows in non-orthogonal coordinates. The basic idea is in using body - fitted - coordinates is to map the complex flow domain in

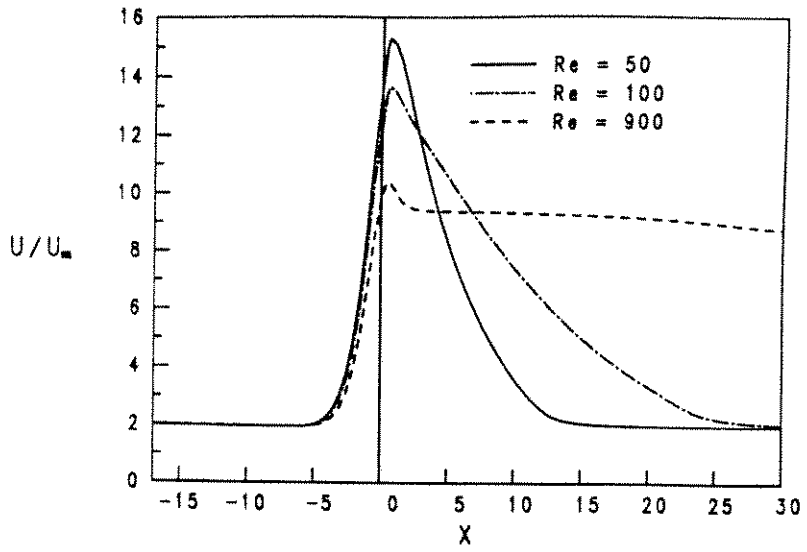

Figure 7: Velocity distribution along the duct.

the physical space to a simple rectangular domain in the computational space by using a curvilinear coordinate transformation. This method also employes collocated variable arrangement and cartesian velocity components. The employment of collocated variables, which means that all variables share the same control volume, has various advantages over the staggered grid. Among them are that the control volumes for all variables coincide with the boundaries of the solution field, facilitating the specification of boundary conditions and a relatively simple extension to general non-orthogonal meshes. The non-physical oscillation in pressure and velocity fields overcome by introducing the Rhie-Chow interpolation procedure. The performance of the method was assessed by computation of flow characteristics through a sever stenosis wich is of physiological interest. Agreement with the available measured data is good. The calculations indicate extended regions of flow recirculation and large values of pressure drop. Both of these phenomena are known as contributing factors in arterial diseases.

References

[1] J. P. van Doormal and G. D. Raithby, *Enhancements of the SIMPLE method for predicting incompressible fluid flows*, Numer. Heat Transfer, Vol. 7, pp. 147-163, 1984.

[2] W. Shyy, S. S. Tong and S. M. Corre, *Numerical Recirculating Flow Calculation Using Body-Fitted Coordinate System*, Numer. Heat Transfer, Vol.8, pp. 99-

113, 1985.

[3] **M. Braaten and W. Shyy,** *Study of Recirculating Flow Computation using Body-Fitted Coordinates: Consistancy Aspects and Mesh Skewness*, **Numer. Heat Transfer, Vol. 9, pp. 559-574, 1986.**

[4] **C. M. Rhie and W. L. Chow,** *Numerical Study of the Turbulent Flow Past an Airfoil with Trailing Edge Separation*, **AIAA J., Vol. 2, pp. 1527-1532, 1983.**

[5] **A. D. Burns and N. S. Wilkes,** *A Finite Difference Method for the Computation of Fluid Flow in Complex Three-Dimensional Geometries*, **AERE R 12342, Harwell Laboratory, U.K., 1986.**

[6] **S. Majumdar** *Developing of a Finite-Volume Procedure for Prediction of Fluid Flow Problems with Complex Irregular Boundaries* **SFB 210/T/29, University of Karlsruhe, 1986.**

[7] **M. Peric. R. Kessler and G. Scheuerer,** *Comparison of Finite-Volume Numerical Methods with Staggered and Collocated grids*, **Comput. Fluids, Vol. 16, pp. 389-403, 1988.**

[8] **T. F. Miller and F. W. Schmidt,** *Use of a Pressure-Weighted Interpolation Method for the Solution of the Incompressible Navier-Stokes Equations on a Non-Staggered System*, **Numer. Heat Transfer, Vol. 14, pp. 213-233, 1988.**

[9] **S. Majumdar,** *Role of Underrelaxtion in Momentum Interpolation for Calculation of Flow with Non-staggered grids*, **Numer. Heat Transfer Vol. 13, pp. 125-132, 1988.**

[10] **B. Van Leer,** *Towards the Altimate Conservative Difference Scheme. II. Monotonocity and Conservation Combined in a Second-Order Scheme*, **J. Comp. Phys. Vol. 14, pp. 361-370, 1974.**

[11] **F. Irgens,** *Tensoranalyse og Kontinumsmekanik. del III*, **Institutt for Mekanikk, Norge Tekniska Hoskole, Trondhiem, 1966.** (in Norwegian)

[12] **S. V. Patankar,** *Numerical Heat Transfer and Fluid Flow* **McGraw-Hill, Washington, 1980.**

[13] **L. Davidson,** *Numerical Simulation of turbulent Flow in Ventilated Rooms*, **PhD thesi. Dept. of Applied Thermodynamics and Fluid Mechanics, Chalmers University of Technology, Göteborg, Sweden, 1989.**

[14] **D. F. Young and F. Y. Tsai,** *Flow characteristics in Models of Arterial Stenoses - I. Steady Flow*, **J. Biomechanics, Vol. 6, pp. 395-410, 1973.**

[15] **K. C. Karki,** *A Calculation Procedure for Viscous Flows at All Speeds in Complex Geometries*, **PhD thesis, University of Minnesota, 1986.**

[16] **M. D. Deshpande, D. P. Giddens, and R. F. Mabon,** *Steady Laminar Flow Through Modelled Vascular Stenoses*, **J. Biomechanics, Vol. 9, pp. 165-174, 1976.**

[17] **A. K. Rastogi,** *Hydrodynamics in Tubes Perturbed by Curvilinear Obstructions*, **J. Fluid Engng., Vol. 106, pp. 262-269, 1984.**

[18] **L. Davidson and P. Hedberg,** *FLUX2D: A Finite-Volume Computer Program Written in General Non-Orthogonal Coordinates for Calculation of Two-Dimensional Turbulent Flow*, **Publication no. 88/1, Dept. of Thermo- and Fluid Dynamics, Chalmers University of Technology, Göteborg, Sweden, 1988.**